

# Stable Cosmic Vortons

Julien Garaud,<sup>1,2</sup> Eugen Radu,<sup>3</sup> and Mikhail S. Volkov<sup>4</sup>

<sup>1</sup>*Department of Physics, University of Massachusetts Amherst, MA 01003 USA.*

<sup>2</sup>*Department of Theoretical Physics, The Royal Institute of Technology, Stockholm, SE-10691 SWEDEN.*

<sup>3</sup>*Institut für Physik, Universität Oldenburg, Postfach 2503 D-26111 Oldenburg, GERMANY.*

<sup>4</sup>*Laboratoire de Mathématiques et Physique Théorique CNRS-UMR 7350, Université de Tours, Parc de Grandmont, 37200 Tours, FRANCE.*

(Dated: January 21, 2018)

We present for the first time solutions in the gauged  $U(1) \times U(1)$  model of Witten describing vortons – spinning flux loops stabilized against contraction by the centrifugal force. Vortons were heuristically described many years ago, however, the corresponding field theory solutions were not obtained and so the stability issue remained open. We construct explicitly a family of stationary vortons characterized by their charge and angular momentum. Most of them are unstable and break in pieces when perturbed. However, thick vortons with small radius preserve their form in the  $3 + 1$  non-linear dynamical evolution. This gives the first ever evidence of stable vortons and impacts several branches of physics where they could potentially exist. These range from cosmology, since vortons could perhaps contribute to dark matter, to QCD and condensed matter physics.

PACS numbers: 11.10.Lm, 11.27.+d, 98.80.Cq

More than 25 years ago Witten introduced the idea of superconducting cosmic strings in the context of a field theory model that can be viewed as a sector of a Grand Unification Theory (GUT) [1]. The model admits classical solutions describing strings (vortices) whose longitudinal current can attain astronomical values (see [2] for a review).

Soon after, it was realized that superconducting strings could form loops whose current would produce an angular momentum supporting them against contraction [3]. If stable, such cosmic vortons should be of considerable physical interest, but until recently it was not clear if vortons are stable or not, since the underlying field theory solutions were not known. Various approximations were used to describe vortons, for example, by viewing them as thin and large elastic rings [4]. It was also realized that objects similar to vortons could potentially exist also in other domains, as for example in condensed matter physics [5], or in QCD [6]. Since superconducting strings exist in the Weinberg-Salam theory [7], vortons are potentially possible also there.

The first field theory solutions describing stationary vortons were found in the global limit of Witten's model, when the gauge fields vanish [8]. These vortons have approximately equal radius and thickness, like a Horn torus. Solutions describing thin and large vortons were later found as well, however, when perturbed, thin vortons turn out to be dynamically unstable and break in pieces [9]. Although discouraging, this result is actually quite natural, since thin vortons can be locally approximated by straight strings, while the latter are known to become unstable for large currents [2].

However, a more close inspection reveals that unstable modes of superconducting strings have a non-zero minimal wavelength [10], as in the case of the Plateau-Rayleigh instability of a water jet [11]. Therefore, imposing periodic boundary conditions with a short enough period should remove all instabilities. As a result, thick vortons made of short string pieces have chances to be stable.

In this letter we present for the first time stationary vorton solutions in the gauged Witten's model, and our vortons are thick. To study their stability, we simulate their full  $3 + 1$  non-linear dynamics in the limit of vanishing gauge couplings. We find that most of them are unstable, however, thick vortons with a large charge and the smallest possible radius are stable. By continuity, it follows that vortons with non-zero but small gauge couplings should be stable as well.

We therefore present the first evidence of stable vortons, whose features turn out to be quite different from those predicted by the effective theories. This can impact several branches of physics where vortons could potentially exist.

**The model of Witten.**– This is a theory of two Abelian vectors  $A_\mu^{(a)}$  interacting with two complex scalars  $\Phi_a$  ( $a = 1, 2$ ) with the Lagrangian

$$\mathcal{L} = -\frac{1}{4} \sum_a F_{\mu\nu}^{(a)} F^{(a)\mu\nu} + \sum_a (D_\mu \Phi_a)^* D^\mu \Phi_a - V. \quad (1)$$

Here the gauge field strengths are  $F_{\mu\nu}^{(a)} = \partial_\mu A_\nu^{(a)} - \partial_\nu A_\mu^{(a)}$ , the gauge covariant derivatives  $D_\mu \Phi_a = (\partial_\mu + ig_a A_\mu^{(a)}) \Phi_a$  with gauge couplings  $g_a$ , and the potential is

$$V = \sum_a \frac{\lambda_a}{4} (|\Phi_a|^2 - \eta_a^2)^2 + \gamma |\Phi_1|^2 |\Phi_2|^2 - \frac{\lambda_2 \eta_2^4}{4}, \quad (2)$$

where  $\eta_1 = 1$ . If  $4\gamma^2 > \lambda_1 \lambda_2$  and  $2\gamma > \lambda_2 \eta_2^2$  then the global minimum of the potential (vacuum) is achieved for  $|\Phi_1| = 1$  and  $\Phi_2 = 0$ . Fields  $A_\mu^{(1)}$ ,  $\Phi_1$ ,  $\Phi_2$  are massive with masses, respectively,  $m_A^2 = 2g_1^2$ ,  $m_1^2 = \lambda_1$ ,  $m_2^2 = \gamma - \frac{1}{2} \lambda_2 \eta_2^2$  whereas  $A_\mu^{(2)}$  is massless and can be identified with electromagnetic field. The theory has a local  $U(1) \times U(1)$  invariance and two Noether currents,  $j_a^\mu = 2\text{Re}(i\Phi_a^* D^\mu \Phi_a)$ , with two conserved charges  $\int j_a^\mu d^3x$ . The Euler-Lagrange equations are

$$\partial_\mu F^{(a)\mu\nu} = g_a j_a^\nu, \quad D_\mu D^\mu \Phi_a + \frac{\partial V}{\partial |\Phi_a|^2} \Phi_a = 0. \quad (3)$$

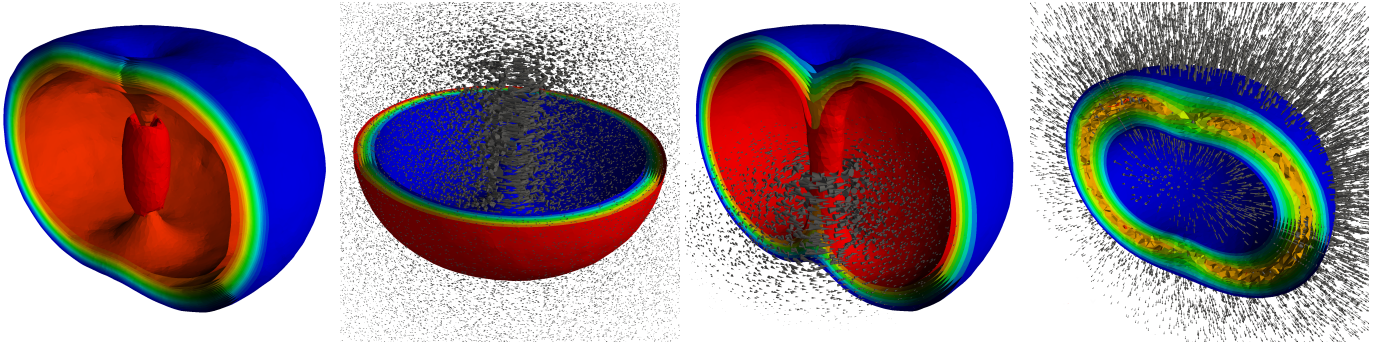


Figure 1. (Color online) – Profiles of the stationary vorton solution for  $Q = 1500$  and  $n = 1, m = 1$  for the parameter values  $\lambda_1 = 41.1$ ,  $(\lambda_2, \eta_2) = (30, 1)$ ,  $\gamma = 20$ , and  $g_1 = g_2 = 0.01$ . The first panel displays constant energy surfaces. The second panel shows surfaces of constant  $|\Phi_1|^2$  and the magnetic field  $\vec{B}^{(1)}$  (cones). One has  $\vec{E}^{(1)} = 0$ . The third panel shows  $|\Phi_2|^2$  isosurfaces and the electromagnetic current  $\vec{j}_2$  (cones). The last panel shows the electric field  $\vec{E}^{(2)}$  (cones), while the isosurfaces show its magnitude. The red color corresponds to large values and the blue color to small values.

Assuming cylindrical coordinates  $x^\mu = (t, \rho, z, \varphi)$ , we make the ansatz for stationary, axially symmetric fields,

$$\Phi_1 = X_1 + iY_1, \Phi_2 = (X_2 + iY_2) \exp\{i(\omega t + m\varphi)\}, \quad (4)$$

where  $X_a, Y_a$  as well as  $A_\mu^{(a)}$  depend on  $\rho, z$ , and we impose the gauge condition  $A_\rho^{(a)} = 0$ . Here  $m$  is an integer winding number and  $\omega$  is a frequency. The fields should be globally regular and the energy should be finite, which requires that at infinity  $X_1 \rightarrow 1$  while all other amplitudes approach zero. At the symmetry axis,  $\rho = 0$ , the amplitudes  $X_2, Y_2, A_\varphi^{(a)}$  vanish, while for the other amplitudes the normal derivative  $\partial/\partial\rho$  vanishes. Under the reflection  $z \rightarrow -z$  the amplitudes  $Y_a$  are odd whereas all the others are even.

The choice of the ansatz implies that the first Noether charge vanishes, while the second one is

$$Q = 2 \int d^3x (X_2^2 + Y_2^2) (\omega - g_2 A_t^{(2)}). \quad (5)$$

The energy is  $E = \int T_t^t d^3x$  and the angular momentum

$$J = \int T_\varphi^t d^3x = mQ, \quad (6)$$

where the energy-momentum tensor is obtained by varying the metric tensor,  $T_\nu^\mu = 2g^{\mu\sigma} \partial\mathcal{L}/\partial g^{\sigma\nu} - \delta_\nu^\mu \mathcal{L}$ . In the above formulas all fields and coordinates are dimensionless. If  $\eta$  is the energy scale, then the dimensionful (boldfaced) quantities are  $\Phi_a = \eta\Phi_a$ ,  $A_\mu^{(a)} = \eta A_\mu^{(a)}$ ,  $x^\mu = \mathbf{x}^\mu \eta$ ,  $\mathbf{E} = \eta E$ , hence  $\eta$  is the asymptotic value of  $\Phi_1$ .

**Stationary vortons.**– Inserting the ansatz (4) to the field equations (3) gives, after separating  $t$  and  $\varphi$  variables, an elliptic system of 10 non-linear PDE's for the 10 functions of  $\rho, z$ . We solve these equations with two different numerical methods: using the elliptic PDE solver FIDISOL based on the Newton-Raphson procedure [12], and also minimizing the energy within a finite element approach provided by the Freefem++ library [13].

We look for solutions with a toroidal structure and non-trivial phase windings along both torus generators. Apart from the azimuthal winding number  $m$ , there is a second integer,  $n$ , determining the winding of phase of  $\Phi_1$  around the boundary of the  $(\rho, z)$  half-plane. If  $n \neq 0$  then  $\Phi_1$  vanishes at a point  $(\rho_0, 0)$  corresponding to the center of the closed vortex forming the vorton, and the phase of  $\Phi_1$  winds around this point. Prescribing non-zero values of  $n, m$ , and  $Q$  (see [14] for details), the fields cannot unwind to vacuum, and the iterative numerical procedure converges to a smooth limiting configuration with a finite radius  $\rho_0$ . We have constructed in this way vortons for  $n = 1, 2$  and  $m = 1, \dots, 12$ , and also solutions similar to Q-balls [15] for  $n = 0, m = 0, 1, \dots$  [14].

The vorton can be visualized as a toroidal tube confining a magnetic flux of  $\vec{B}^{(1)} = \vec{\nabla} \times \vec{A}^{(1)}$ , since  $\Phi_1 \approx 0$  inside the tube and thus the first U(1) is restored.  $\Phi_2$  is non-zero inside the tube, giving rise to a charged condensate and to a persistent electric current along the tube. The current creates a momentum along the azimuthal direction, which gives rise to an angular momentum along  $z$ -direction. Outside the vorton tube the massive fields  $A_\mu^{(1)}, \Phi_1, \Phi_2$  rapidly approach their vacuum values and there remains only the long-range massless  $A_\mu^{(2)}$  generated by the electric current confined inside the vorton tube. At large  $r = \sqrt{\rho^2 + z^2}$  one has  $A_t^{(2)} = Q/(4\pi r) + \dots$  and  $A_\varphi^{(2)} = \mu \sin\theta/r^2 + \dots$ , therefore, from far away the vorton looks like a superposition of an electric charge  $Q$  with a magnetic dipole  $\mu$ .

Fig. 1 shows the 3D solution profiles for an  $m = 1$  vorton. One can see that the vorton tube is very thick and compact. The vortex magnetic field  $\vec{B}^{(1)} = \vec{\nabla} \times \vec{A}^{(1)}$  and the electric current  $\vec{j}_2$  are tangent to the azimuthal lines. The electric field  $\vec{E}^{(2)} = -\vec{\nabla} A_t^{(2)}$  is mostly oriented along the radial direction and supports a non-zero flux at infinity,  $\mathcal{Q} = \oint d\vec{E}^{(2)} \cdot d\vec{S} = g_2 Q$ . The massless magnetic field  $\vec{B}^{(2)} = \vec{\nabla} \times \vec{A}^{(2)}$  at large  $r$  is of magnetic dipole type.

Vortons can be labelled by their charge  $Q$  and the integer ‘spin’  $m = J/Q$  (assuming that  $n = 1$ ). The vorton radius

$\rho_0$  is not very sensitive to the value of  $Q$  but increases rapidly with  $m$ , so that for large  $m$  vortons are thin and large, with the radius much larger than the thickness. On the other hand, increasing  $Q$  increases the thickness of the vorton tube, so that for large  $Q$  vortons are thick and look almost spherical.

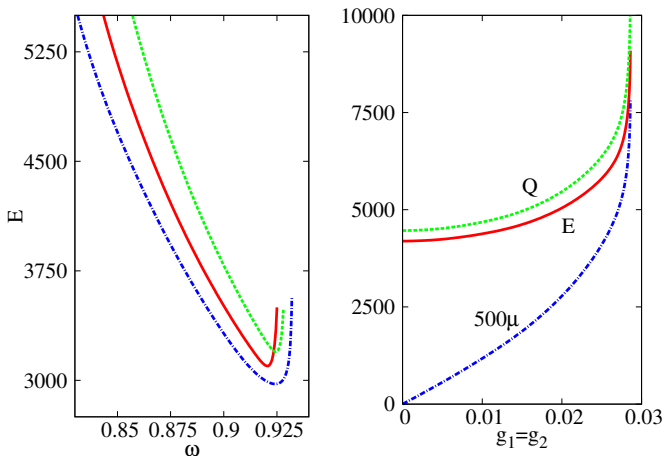


Figure 2. (Color online) – Left panel shows  $E$  against  $\omega$  for the values of gauge couplings  $(g_1, g_2) = (0.008, 0.021)$  (dashed),  $(0.012, 0.012)$  (solid),  $(0.008, 0.027)$  (dotted). Right panel shows  $E$ ,  $Q$ ,  $\mu$  against  $g_1 = g_2$  for a fixed  $\omega = 0.804$ . In both cases  $\lambda_1 = 41.1$ ,  $\lambda_2 = 40$ ,  $\gamma = 22.3$ ,  $\eta_2 = 1$ ,  $n = 1$ ,  $m = 2$ .

The frequency  $\omega$  can be used instead of  $Q$  to characterize the solutions, which exist only within a finite frequency range,  $\omega_- < \omega < \omega_+$ . Both  $E$  and  $Q$  diverge for  $\omega \rightarrow \omega_{\pm}$  and have a minimum in between, as shown in Fig. 2. Vortons can be viewed as boson condensates, which is why their charge cannot be too small, since the boson condensation is not energetically favoured for small quantities of the field quanta.

For  $g_a = 0$  the gauge fields vanish and the vortons are global, ‘made of’ the scalars  $\Phi_a$  alone [8]. For  $g_a \neq 0$  the gauge fields are excited and increase the total energy and charge, as shown in Fig. 2. Solutions do not exist for arbitrary values of  $\lambda_a, \eta_2, \gamma, g_a$  but only for some regions in the parameter space. For example, fixing all parameters and also  $\omega$  and varying  $g_1 = g_2$ , the solutions exist only within a finite range of gauge couplings, as is seen in Fig. 2.

**Dynamical vortons.**– To analyze the vorton stability, we simulate their non-linear  $3 + 1$  temporal dynamics. In doing this, we consider only the global vortons, since simulating dynamics of the gauge fields would require too much computer power. However, we expect the results obtained in the global case to apply to the fully gauged vortons as well, at least for small enough gauge couplings  $g_a$ . Indeed, for  $g_a = 0$  the vorton is made of scalars  $\Phi_a$ . For small nonzero  $g_a$  their global currents give rise to the  $O(g_a)$  source in the gauge field equations, hence  $A_{\mu}^{(a)} = O(g_a)$ . The backreaction of the gauge fields on the scalars is  $O(g_a^2)$  and can be neglected as compared to the reaction of the scalars on themselves. For stationary vortons this is confirmed by the numerics, as is seen in Fig. 2. Therefore, one can expect the temporal dynamics

of vortons with small  $g_a$  to be dominated by the scalars only, hence it can be approximated by the global vorton dynamics.

Vortons with large  $m$  develop pinching deformations breaking them in pieces [9]. However, for small  $m$ , vortons could be stable, since they are compact and thick and have no room for the instability to settle in. To verify this, we consider a hyperbolic evolution scheme based on an implicit  $\beta$ -Newmark finite difference approximation (see [14] for details). The initial configuration is a stationary, axially symmetric vorton. It becomes automatically perturbed by the space discretization when adapted from 2D to the 3D mesh, which triggers a non-trivial temporal evolution. The natural timescale is set by the value of  $\omega$  of the underlying vorton solution, which is of order one. We integrate with the timestep  $\Delta t = 0.1$  and find that the  $m \geq 3$  vortons very quickly become strongly deformed and then break in pieces. The time they take to break decreases rapidly as  $m$  grows (see Fig. 3 and [14] for the videos). The products of the vorton decay are typically two or three outspiralling fragments of spherical topology.

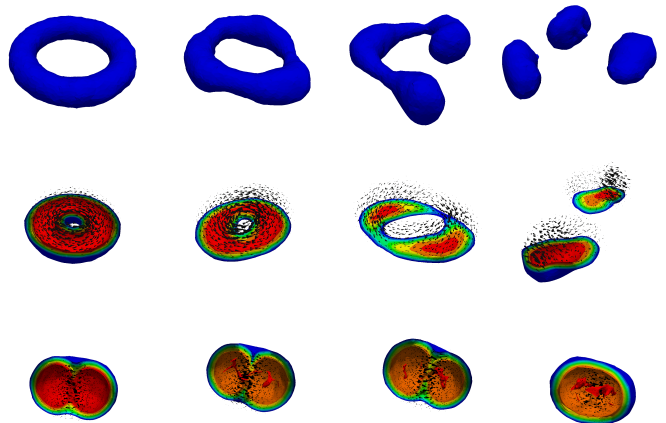


Figure 3. (Color online) – Snapshots of the vorton time evolution. The first line shows a constant  $|\Phi_2|^2$  surface for the  $m = 6$  solution for  $t = 0, 17, 21, 28$ . The second and third lines show the constant  $|\Phi_1|^2$  surfaces and the electric current, respectively, for  $m = 3$  vorton for  $t = 0, 31, 28, 47$  and for the  $m = 1$  vorton for  $t = 0, 104, 153, 239$ . The third line shows the stable solution for  $Q = 6000$  and for the same values of  $\lambda_a, \eta_2, \gamma$  as in Fig. 2.

We therefore conclude that thin and large vortons are unstable, thus confirming the result of [9]. One should say that a different conclusion was previously made in Ref. [16], where thin vortons were found to be stable. Since neither our analysis nor that of [9] confirm this, it is possible that the conclusion of [16] is an artefact of modifying the scalar potential made in that work in order to improve the stability behavior.

We finally turn to vortons with  $m = 1, 2$  and choose a large value  $Q$ , in which case the vortons are compact and thick. For  $m = 2$  we cannot make a definite conclusion, since the vortons do not actually break but sometimes become strongly deformed. However, nothing at all happens to the

$m = 1$  vortons. As the time goes, they only move slowly in the box, sometimes reflecting from the boundary, without changing shape. We integrated up to  $t \sim 10^3$  (which requires weeks of runtime) without noticing any change in their behavior. We also checked that increasing the size of the box does not change anything, so that one cannot say that the boundary has a stabilizing effect. We therefore conclude that vortons with the lowest ‘spin’ and a large charge are dynamically stable (see [14] for more discussion). Intuitively, this is because they are so thick that they are ‘hard to pinch’.

Interestingly, a very similar conclusion was made for the ‘spinning light bullets’ which share many properties with vortons [17]. These are non-relativistic solutions for a complex scalar field with a  $t, \varphi$ -dependent phase (like for  $\Phi_2$ ), and they also have toroidal profiles. Their  $E(\omega)$  dependence is similar to that shown in Fig. 2. It was found that the  $m = 1$  solutions with a large charge and  $\omega$  close to  $\omega_-$  preserve their shape in the  $3 + 1$  dynamical evolution [17]. Exactly the same statement applies for our relativistic vortons.

In summary, for the first time since the vortons were heuristically described almost 25 year ago [3], we present the underlying stable solutions within the  $U(1) \times U(1)$  gauge field theory of Witten [1]. We can now make some estimates. Assuming the original motivation of Witten, the energy scale should be of the GUT magnitude,  $\eta \sim 10^{14}$  GeV. Using the value  $E \sim 5 \times 10^3$  for estimates, it follows that vortons are extremely heavy, with  $\mathbf{E} \sim 5 \times 10^{17}$  GeV, which is not far from the Planck energy. On the other hand, their minimal Noether charge  $Q \sim 5 \times 10^3$  is actually not so large as compared to the average particle density in the hot early universe. Therefore, vortons could be abundantly created due to charge fluctuations in the course of a phase transition via the Kibble mechanism [18], if only GUTs indeed applied in the past. Being classically stable, vortons could disintegrate via a quantum tunnelling towards the  $\rho_0 = 0$  state, but this process should be exponentially suppressed, and in fact quantum fluctuations can also have a stabilizing effect by preventing the collapse to zero size [19]. Vortons could probably evaporate via interactions with GUT fermions [20], but this process should stop after the GUT epoch. Therefore, it is not inconceivable that some relic vortons could still be around and contribute to dark matter.

Let us consider  $g_a = 0$  vortons. For stationary fields (4), Eqs.(3) for  $\Phi_a$  can formally be interpreted [8] as the non-relativistic Gross-Pitaevskii equation for a two-component Bose-Einstein condensate (BEC). This can describe ultracold atomic gases with two hyperfine states, such as  $^{87}\text{Rb}$  [21]. Scalars  $\Phi_a$  then correspond to the two BEC order parameters, one of which creates a vortex while the other one condenses in the vortex core. Our solutions therefore describe stationary vortons made of loops of such vortices, whose potential existence has been much discussed [5]. In fact, vortex rings in two-component BECs have been observed experimentally [22], although it is not completely clear if they support an angular momentum [23].

$\Phi_1$  and  $\Phi_2$  can also be interpreted [24], respectively, as the

$d$ -wave superconducting (dSC) and antiferromagnetic (AF) order parameters in the  $SO(5)$  model of high  $T_c$  superconductivity [25]. This model admits dSC vortices with an AF core [26], while our solutions describe loops made of these vortices. Such vorton quasiparticles could be important for the superconducting phase transition in this model [24].

Equally, scalars  $\Phi_a$  can be viewed as describing a condensate of  $(K^+, K^0)$  mesons in QCD [27], hence our solutions describe the  $K$ -vortons, whose existence was conjectured in [6]. Setting the scale to be  $\eta \sim 200$  MeV gives for their energy  $\mathbf{E} \sim 1$  TeV. Such objects could probably exist in dense QCD matter, as for example in neutron stars [28], which may affect their electromagnetic and neutrino transport properties.

J.G. was supported by the NSF grant No. DMR-0955902 and by the Swedish Research Council. A part of this work was performed at the Royal Institute of Technology on resources provided by the Swedish National Infrastructure for Computing at the National Supercomputer Center in Linköping, Sweden. E.R. gratefully acknowledges support by the DFG.

- 
- [1] E. Witten, *Nucl. Phys.* **B249**, 557 (1985).
  - [2] A. Vilenkin and E. Shellard, *Cosmic Strings and Other Topological Defects* (Cambridge University Press, 2000).
  - [3] R. L. Davis and E. P. S. Shellard, *Nucl. Phys.* **B323**, 209 (1989).
  - [4] B. Carter, *Phys.Lett.* **B238**, 166 (1990).
  - [5] R. A. Battye, N. R. Cooper, and P. M. Sutcliffe, *Phys. Rev. Lett.* **88**, 080401 (2002); E. Babaev, *Phys. Rev. Lett.* **88**, 177002 (2002); C. M. Savage and J. Ruostekoski, *Phys. Rev. Lett.* **91**, 010403 (2003); M. A. Metlitski and A. R. Zhitnitsky, *JHEP* **06**, 017 (2004).
  - [6] K. B. W. Buckley, M. A. Metlitski, and A. R. Zhitnitsky, *Phys.Rev.* **D68**, 105006 (2003).
  - [7] J. Garaud and M. S. Volkov, *Nucl. Phys.* **B826**, 174 (2010).
  - [8] E. Radu and M. S. Volkov, *Phys. Rept.* **468**, 101 (2008).
  - [9] R. A. Battye and P. M. Sutcliffe, *Nucl. Phys.* **B814**, 180 (2009).
  - [10] J. Garaud and M. S. Volkov, *Nucl. Phys.* **B839**, 310 (2010); *Nucl. Phys.* **B799**, 430 (2008).
  - [11] J. Eggers, *Rev. Mod. Phys.* **69**, 865 (1997).
  - [12] W. Schönauer and E. Schnepf, *ACM Trans. Math. Softw.* **13**, 333 (1987).
  - [13] F. Hecht, O. Pironneau, A. Le Hyaric, and K. Ohtsuka, *The Freefem++ manual* (2007).
  - [14] See Appendix for more details and technical discussion. Videos of the dynamical evolution are available online at <http://people.umass.edu/garaud/Webpage/vortons.html>.
  - [15] K.-M. Lee, J. A. Stein-Schabes, R. Watkins, and L. M. Widrow, *Phys. Rev.* **D39**, 1665 (1989).
  - [16] Y. Lemperiere and E. P. S. Shellard, *Phys. Rev. Lett.* **91**, 141601 (2003).
  - [17] D. Mihalache, D. Mazilu, L.-C. Crasovan, I. Towers, A. V. Buryak, B. A. Malomed, L. Torner, J. P. Torres, and F. Lederer, *Phys. Rev. Lett.* **88**, 073902 (2002).
  - [18] J. A. Frieman, G. B. Gelmini, M. Gleiser, and E. W. Kolb, *Phys. Rev. Lett.* **60**, 2101 (1988); K. Griest, E. W. Kolb, and A. Massarotti, *Phys. Rev. D* **40**, 3529 (1989).
  - [19] M. Quandt, N. Graham, and H. Weigel, *Phys. Rev. D* **87**, 085013 (2013).
  - [20] A. Kusenko and M. E. Shaposhnikov, *Phys.Lett.* **B418**, 46

- (1998).
- [21] C. J. Myatt, E. A. Burt, R. W. Ghrist, E. A. Cornell, and C. E. Wieman, *Phys.Rev.Lett.* **78**, 586 (1997); D. S. Hall, M. R. Matthews, C. E. Wieman, and E. A. Cornell, *Phys. Rev. Lett.* **81**, 1543 (1998).
- [22] B. P. Anderson, P. C. Haljan, C. A. Regal, D. L. Feder, L. A. Collins, C. W. Clark, and E. A. Cornell, *Phys. Rev. Lett.* **86**, 2926 (2001).
- [23] M. Nitta, K. Kasamatsu, M. Tsubota, and H. Takeuchi, *Phys. Rev. A* **85**, 053639 (2012).
- [24] K. B. W. Buckley and A. R. Zhitnitsky, *Phys.Rev.* **B67**, 174522 (2003).
- [25] S. Zhang, *Science* **21**, 1089 (1997).
- [26] D. P. Arovas, A. J. Berlinsky, C. Kallin, and S.-C. Zhang, *Phys. Rev. Lett.* **79**, 2871 (1997); S. Alama, A. J. Berlinsky, L. Bronsard, and T. Giorgi, *Phys. Rev. B* **60**, 6901 (1999).
- [27] D. B. Kaplan and S. Reddy, *Phys.Rev.Lett.* **88**, 132302 (2002).
- [28] K. B. W. Buckley, M. A. Metlitski, and A. R. Zhitnitsky, *Phys.Rev.Lett.* **92**, 151102 (2004); *Phys. Rev. C* **69**, 055803 (2004).

## APPENDIX

We used three completely different numerical techniques for the vorton construction. First, we performed our calculations using the elliptic PDE solver FIDISOL based on the iterative Newton-Raphson method [12] within a finite difference scheme. This method solves the equations of motion for the stationary, axially symmetric fields. To construct a solution with this method, one fixes the values of the winding

numbers  $n, m$  and also the frequency  $\omega$  in the ansatz (A.2), whereas  $Q$  is obtained from Eq.(A.8). This method requires a good choice of the starting field configuration. Next, we reproduced the same solutions using the energy minimization scheme within a finite element framework provided by the Freefem++ library [13]. In this case the input parameters are  $n, m, Q$ , while  $\omega$  is obtained from (A.10). This method is less sensitive to the choice of the input field configuration. Finally, we simulated the hyperbolic evolution of the full 3 + 1 theory, also using the Freefem++ library [13]. Below we shall describe the two last methods.

### Energy minimization

The energy-momentum tensor of Witten's model is

$$T_{\nu}^{\mu} = - \sum_a F^{(a)\mu\rho} F_{\nu\rho}^{(a)} + \sum_a (D^{\mu}\Phi_a)^* D_{\nu}\Phi_a + \sum_a (D_{\nu}\Phi_a)^* D^{\mu}\Phi_a - \delta_{\nu}^{\mu}\mathcal{L}, \quad (\text{A.1})$$

and the energy  $E = \int T_t^t d^3x$ . Using the axially symmetric ansatz in the radial gauge,

$$A_{\mu}^{(a)} dx^{\mu} = V^{(a)} dt + W^{(a)} d\varphi + Z^{(a)} dz, \quad (\text{A.2})$$

$$\Phi_1 = X_1 + iY_1, \quad \Phi_2 = (X_2 + iY_2) \exp\{i(\omega t + m\varphi)\},$$

where  $X_a, Y_a, V^{(a)}, W^{(a)}, Z^{(a)}$  depend on  $\rho, z$ , gives

$$E = \int \left\{ \frac{1}{2} \sum_a \left( \nabla V^{(a)2} + \frac{1}{\rho^2} \nabla W^{(a)2} + \partial_{\rho} Z^{(a)2} \right) + 2 \sum_a g_a Z^{(a)} (Y_a \partial_z X_a - X_a \partial_z Y_a) + \nabla X_1^2 + \nabla Y_1^2 + \nabla X_2^2 + \nabla Y_2^2 + \left( (g_1 V^{(1)})^2 + \left( \frac{g_1}{\rho} W^{(1)} \right)^2 + (g_1 Z^{(1)})^2 \right) (X_1^2 + Y_1^2) + \frac{\lambda_1}{4} (X_1^2 + Y_1^2 - \eta_1^2)^2 + \gamma (X_1^2 + Y_1^2) (X_2^2 + Y_2^2) + \left( (\omega - g_2 V^{(2)})^2 + \frac{1}{\rho^2} (m - g_2 W^{(2)})^2 + (g_2 Z^{(2)})^2 + \frac{\lambda_2}{4} (X_2^2 + Y_2^2 - 2\eta_2^2) \right) (X_2^2 + Y_2^2) \right\} d^3x, \quad (\text{A.3})$$

where  $\nabla \equiv (\partial_{\rho}, \partial_z)$  denotes the gradient operator in the  $(\rho, z)$ -plane. Since the integrand in (A.3) does not depend on  $\varphi$  and is invariant under  $z \rightarrow -z$ , we choose the integration domain to be a quadrant of radius  $r_{\max}$ ,

$$\Omega := \left\{ \rho, z \in [0, r_{\max}] \times [0, r_{\max}] \mid \sqrt{\rho^2 + z^2} \leq r_{\max} \right\}, \quad (\text{A.4})$$

this is illustrated in Fig. 4. Regularity conditions at the symmetry axis require that at  $\rho = 0$  one has

$$X_2 = Y_2 = 0, \quad \partial_{\rho} X_1 = \partial_{\rho} Y_1 = 0, \\ W^{(a)} = 0, \quad \partial_{\rho} V^{(a)} = \partial_{\rho} Z^{(a)} = 0. \quad (\text{A.5})$$

The reflexion symmetry in the equatorial plane implies that at  $z = 0$

$$\partial_z X_a = 0, \quad Y_a = 0, \\ \partial_z V^{(a)} = \partial_z W^{(a)} = \partial_z Z^{(a)} = 0. \quad (\text{A.6})$$

Since the massive fields approach their asymptotic values exponentially fast, we assume that for  $\sqrt{\rho^2 + z^2} = r_{\max}$  the fields take on the vacuum values

$$X_1 = 1, \quad Y_1 = X_2 = Y_2 = 0, \quad \text{and} \quad A_{\mu}^{(a)} = 0, \quad (\text{A.7})$$

but then we refine this by imposing mixed boundary conditions for the massless  $A_{\mu}^{(2)}$  to take into account its slow falloff.

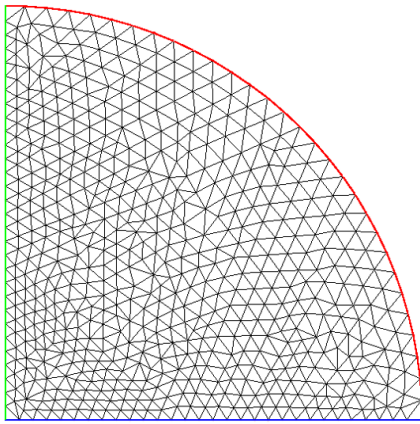


Figure 4. (Color online) – Triangulation over the computational domain.

We find stationary solutions by minimizing the energy for a fixed Noether charge  $Q$ . To this end, we express the frequency  $\omega$  in terms of  $Q$  via rewriting (5) of the main text, in the form

$$Q = 2(\omega\Sigma_1 - \Sigma_2) \quad (\text{A.8})$$

with

$$\begin{aligned} \Sigma_1 &= \int d^3x (X_2^2 + Y_2^2), \\ \Sigma_2 &= \int d^3x g_2 V^{(2)}(X_2^2 + Y_2^2), \end{aligned} \quad (\text{A.9})$$

so that

$$\omega = \frac{Q + 2\Sigma_2}{2\Sigma_1}, \quad (\text{A.10})$$

which should be inserted to (A.3). The energy is then minimized at a fixed  $Q$ .

Having fixed  $Q$ , one has to fix also the winding numbers  $n, m$ . The number  $m$  determines the windings of the phase of  $\Phi_2 \sim e^{im\varphi}$  along the azimuthal direction, and, after separating the angular variable, is explicitly contained in the integrand in (A.3). The number  $n$  determines the increase of phase of  $\Phi_1 = X_1 + iY_1$  around the boundary of  $(\rho, z)$  half-plane. To fix it, one chooses  $X_1(\rho, z)$  and  $Y_1(\rho, z)$  which vanish, respectively,  $n$  and  $n - 1$  times along the positive  $z$ -axis, for  $\rho = 0$  and  $0 < z < \infty$  [8]. This guarantees that  $\Phi_1$  vanishes at a point  $(\rho_0, 0)$  corresponding to the center of the closed vortex forming the vorton, and the phase of  $\Phi_1$  winds around this point. It is sufficient to enforce the value of  $n$  only for the input  $X_1, Y_1$  field configuration, since later it will be automatically preserved in the energy minimizing iterations (unless the vortex center hits the  $z$ -axis), because ‘unwinding’ would require an infinite amount of energy.

After fixing  $Q, m$  in (A.3) and choosing an input configuration  $X_1(\rho, z), Y_1(\rho, z), X_2(\rho, z)$  with the prescribed value of  $n$ , the iterative energy minimization produces a sequence

of regular, vorton-type configurations. However, these do not necessarily converge to a smooth limiting configuration, even though the energy is bounded from below. If  $Q$  is small, then the values of  $\rho_0$  typically converge to zero and the vorton loops shrink. Physically, this means that there are not enough field quanta to condense and make a vorton. There are no stationary solutions in this case and the stationary energy minimizer is trying to approximate a non-stationary collection of non-condensed quanta. On the other hand, for a large enough  $Q$  the  $\rho_0$ -values converge to a finite limit corresponding to the radius of the stationary vorton.

The variational problem of minimizing (A.3) is defined for numerical computations by adapting a finite element formulation provided by the Freefem++ library [13]. The discretization within this formulation is done via a (homogeneous) triangulation over  $\Omega$ , based on the Delaunay-Voronoi algorithm. The functions are expanded with respect to a continuous piecewise quadratic polynomial basis on each triangle. The accuracy of the method is controlled by the number of triangles, by the order of expansion in the basis for each triangle, and also by the order of the quadrature formula for the integral over the triangles. Once the problem is mathematically posed, a numerical optimization algorithm is used to solve the nonlinear variational problem of finding the minima of  $E$ . We used a nonlinear conjugate gradient method. The algorithm is iterated until the relative variation of the norm of the gradient of the functional  $E$  with respect to all degrees of freedom is less than  $10^{-6}$ . Virial relations which should be fulfilled by the solutions are then checked.

### Q-balls versus Vortons

One can consistently set to zero in the field equations the imaginary part of the first scalar and the first gauge field,  $Y_1 = \text{Im}(\Phi_1) = 0, A_\mu^{(1)} = 0$ . Solutions obtained in this case are similar to the gauged Q-balls described in [15].  $\Phi_1$  is then real and has no phase winding ( $n = 0$ ), while  $\Phi_2 \sim e^{im\varphi}$  remains complex-valued. Q-balls with  $m = 0$  are spherically symmetric and non-spinning, while those with  $m \neq 0$  are axially symmetric and support a non-zero angular momentum  $J = mQ$ . Spinning Q-balls have toroidal profiles similar to those for vortons. For Q-balls the field  $\Phi_1$  is small inside the torus tube, although it does not vanish at the center of the tube as for vortons. Since  $\Phi_1$  is real, the first Noether current  $j_1^\mu$  vanishes, and there is no flux of  $\vec{B}^{(1)}$  along the torus tube. However, for Q-balls as for vortons, the phase of  $\Phi_2$  winds along the torus tube giving rise to an azimuthal current  $j_2^\mu$  and to a dipole magnetic field  $\vec{B}^{(2)}$ . Both Q-balls and vortons carry an electric charge  $Q = \oint d\vec{E}^{(2)} \cdot d\vec{S} = g_2 Q$ . For a given (large enough) charge  $Q$  and an azimuthal winding number  $m$ , Q-balls and vortons have the same angular momentum  $J = mQ$ . However, their energies  $E$  are not the same, Q-balls being less energetic (see Fig. 5). Therefore, vortons are not energetically protected from decaying into Q-balls, although

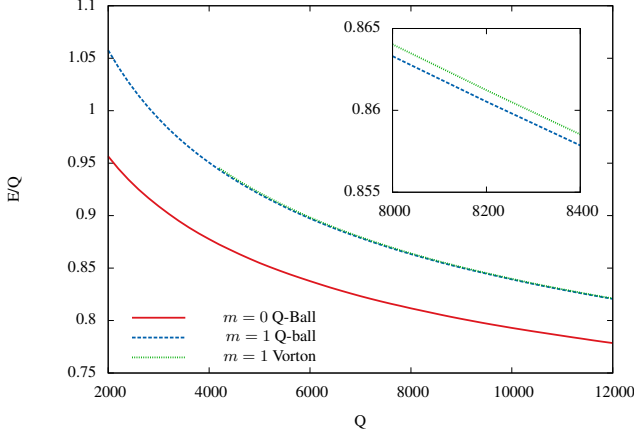


Figure 5. (Color online) – The energy-to-charge ratio  $E/Q$  against  $Q$  for Q-balls and vortons for the same parameters as in Fig. 1 in the main text. The lower (red) curve corresponds to the  $m = 0$  Q-balls. The upper (blue-green) curve corresponds to the  $m = 1$  Q-balls and vortons whose energies turn out to be almost the same. Zooming this curve shown in the insertion reveals that the vorton energy (dotted green line) is slightly larger than the Q-ball energy (dashed blue line).

they cannot decay into free particles (since  $E/Q < 1$ ).

The lightest solution for a given  $Q$  is the spherically symmetric Q-ball with  $J = 0$ , but vortons cannot decay to it due to the angular momentum conservation, unless they break in several components spiralling around the total center of mass. It seems this is exactly what happens for the  $m > 2$  vortons, as described in the main text. Specifically, they seem to unwind to  $n = 0$  via shrinking the  $\Phi_1 = 0$  line to zero and split into small spherical Q-balls whose total orbital angular momentum equals the initial  $J$ .

However, the  $m = 1$  vorton is ‘hard to pinch’ and it does not break into non-spinning Q-balls. On the other hand, it could in principle decay into the  $m = 1$  spinning Q-ball with the same  $Q, J$ , although their relative energy difference is only  $\sim 10^{-3}$  (see Fig. 5). To unwind to the Q-ball, the vorton has to get rid of the phase winding around the closed line where  $\Phi_1 = 0$ . This line cannot break, since this would cost an infinite energy, but it can shrink to zero at a finite energy cost. To estimate the energy needed, we considered an interpolating sequence of trial field configurations for which  $A_\mu^{(a)}$  and  $\Phi_2$  are the same as for the  $m = 1$  stationary vorton, while  $\Phi_1(x^\mu)$  is replaced by  $\Phi_1(\lambda x^\mu)$  with  $\lambda$  being the scale parameter. We then calculate the total energy  $E(\lambda)$ , which coincides with the vorton energy for  $\lambda = 1$ . The  $\Phi_1 = 0$  line shrinks to zero when  $\lambda \rightarrow \infty$ , and it turns out that  $E(\infty) \approx 3 \times E(1)$ , which gives an idea of the energy needed to unwind. Therefore,  $m = 1$  vortons and Q-balls are separated by a potential barrier whose height is of the same order as the vorton energy. Since vortons are rather heavy, a very strong perturbation is needed to unwind them into Q-balls. As mentioned in the main text, the vorton unwinding could also be disfavoured by quantum effects.

The conclusion is that the  $m = 1$  vortons are dynamically stable and could, perhaps, be destroyed only by very strong perturbations.

### Hyperbolic evolution

To investigate the dynamical stability of the global vortons, the axially symmetric solutions are used as the initial data for a  $3 + 1$  evolution code. This time the integration domain  $\Omega$  is an (open) bounded subset of  $\mathbb{R}^3$  with the boundary  $\partial\Omega$  and with the attached normal derivative  $\partial_n$ . We choose  $\Omega$  to be the interior of a sphere of radius  $r_{\max}$ . The discrete version is obtained by a homogeneous triangulation over  $\Omega$ . The following numerical scheme was used to evolve the vortons. The dynamical equations for the scalars read in the global limit

$$\partial_{tt}\Phi_a - \Delta\Phi_a + \frac{\partial V}{\partial|\Phi_a|^2}\Phi_a = 0. \quad (\text{A.11})$$

Here  $\Delta \equiv \vec{\nabla}^2$  is the Laplace operator and  $\vec{\nabla}$  the gradient operator in three space dimensions in Cartesian coordinates. The weak formulation of the hyperbolic problem (A.11) is obtained by multiplying the equation by test functions  $w_a$ , integrating over  $\Omega$  and applying the Stokes formula,

$$\int_{\Omega} w_a \partial_{tt}\Phi_a + \int_{\Omega} \vec{\nabla} w_a \cdot \vec{\nabla}\Phi_a + \int_{\Omega} w_a \frac{\partial V}{\partial|\Phi_a|^2}\Phi_a - \int_{\partial\Omega} w_a \partial_n \Phi_a = 0. \quad (\text{A.12})$$

The time discretization is achieved using a  $\beta$ -Newmark scheme, which converts (A.12) to

$$\int_{\Omega} w_a \frac{\Phi_a^{[n+1]} - 2\Phi_a^{[n]} + \Phi_a^{[n-1]}}{dt^2} + \int_{\Omega} \vec{\nabla} w_a \cdot \vec{\nabla} \left( \beta\Phi_a^{[n+1]} + (1-2\beta)\Phi_a^{[n]} + \beta\Phi_a^{[n-1]} \right) + \int_{\Omega} w_a \frac{\partial V^{[n]}}{\partial|\Phi_a|^2}\Phi_a^{[n]} - \int_{\partial\Omega} w_a \partial_n \Phi_a^{[n]} = 0, \quad (\text{A.13})$$

where  $\Phi_a^{[n]}, V^{[n]}$  are the value of  $\Phi_a, V$  at the time moment  $t_0 + ndt$ . Here  $0 \leq \beta \leq 1$  and the scheme is unconditionally stable for  $\beta \geq 1/4$ . Typically we choose  $\beta = 1/4$ , which corresponds to the constant average acceleration method, while choosing  $\beta = 1/2$  would reproduce the Crank-Nicholson scheme. We assume that  $\partial_t \Phi_a = 0$  at  $\partial\Omega$ , so that the boundary values of fields are frozen.

The time-discretized equations (A.13) can be rewritten as a recurrence

$$u^{[n+1]} = \mathbf{A}^{-1} \left( \mathbf{B}u^{[n]} + \mathbf{C} \right) - u^{[n-1]} \quad (\text{A.14})$$

where  $u^{[n]} \equiv \{u_i^{[n]}\}$  is the vector containing all discretized degrees of freedom at the  $n$ -th time step.  $\mathbf{A}, \mathbf{B}$  are matrix

bilinear operators and  $\mathbf{C}$  is a vector containing the nonlinearities,

$$\begin{aligned} \mathbf{A}_{ij} &= \int_{\Omega} (u_j^{[n]} u_i^{[n]} + \beta_1 \vec{\nabla} u_j^{[n]} \cdot \vec{\nabla} u_i^{[n]}) - \int_{\partial\Omega} \beta_1 u_j^{[n]} \partial_n u_i^{[n]}, \\ \mathbf{B}_{ij} &= \int_{\Omega} (2u_j^{[n]} u_i^{[n]} - \beta_2 \vec{\nabla} u_j^{[n]} \cdot \vec{\nabla} u_i^{[n]}) + \int_{\partial\Omega} \beta_2 u_j^{[n]} \partial_n u_i^{[n]}, \\ \mathbf{C}_i &= -dt^2 \int_{\Omega} u_i^{[n]} \frac{\partial V^{[n]}}{\partial |\Phi_a^{[n]}|^2} \Phi_a^{[n]}, \end{aligned} \quad (\text{A.15})$$

with  $\beta_1 = \beta dt^2$  and  $\beta_2 = (1 - 2\beta)dt^2$ . Using the stationary, axially symmetric solutions obtained by minimizing the energy, the recurrence is initialized by

$$\begin{aligned} \Phi_1^0 &= X_1(\rho, |z|) + i \operatorname{sg}(z) Y_1(\rho, |z|), & \Phi_1^1 &= \Phi_1^0 \\ \Phi_2^0 &= (X_2(\rho, |z|) + i \operatorname{sg}(z) Y_2(\rho, |z|)) e^{im\varphi}, & \Phi_2^1 &= \Phi_2^0 e^{i\omega dt}. \end{aligned} \quad (\text{A.16})$$

The time step  $dt$  is typically chosen to be 0.1 and the configuration is evolved for several hundreds of internal periods  $T = 2\pi/\omega$ .

It should be stressed that the passage from the stationary, axially symmetric vortons to their dynamical counterparts starts by uplifting the former from two to three spatial dimensions. In doing this, the stationary solutions obtained on the 2D mesh of the type shown in Fig. 4 are interpolated to adapt them to a 3D mesh built via a 3D triangulation over the 3D integration region. The two meshes are completely different and have neither common symmetries nor shared vertices. The uplifted to 3D field configurations thus differ from the very beginning from the true 3D stationary solutions. They correspond instead to perturbed stationary solutions, and it is this initial perturbation which triggers a non-trivial temporal dynamics. The perturbation turns out to be strong enough to destroy the  $m > 2$  vortons almost immediately. Therefore, since the  $m = 1$  vortons survive, this strongly suggests that they are dynamically stable.